Comptes rendus - Geoscience 351 (2019) 551–561

Contents lists available at ScienceDirect

Comptes rendus - Geoscience

www.journals.elsevier.com/comptes-rendus-geoscience

Petrology, Geochemistry

Titanite: A potential solidus barometer for granitic magma systems

Saskia Erdmann [a, b, *], Rucheng Wang [a], Fangfang Huang [a, b], Bruno Scaillet [b], Kai Zhao [a], Hongsheng Liu [a, b], Yan Chen [b], Michel Faure [b]

[a] State Key Laboratory for Mineral Deposit Research, School of Earth Sciences and Engineering, Nanjing University, China
[b] Université d'Orléans, CNRS/INSU – ISTO – BRGM, UMR 7327, Orléans, France

ARTICLE INFO

Article history:
Received 12 September 2018
Accepted 23 September 2019
Available online 15 November 2019
Handled by François Chabaux

Keywords:
Titanite
Amphibole
Barometer
Pressure
Granite

ABSTRACT

Constraining crystallization pressure and thus intrusion depth of granites in various geodynamic settings remains challenging, yet important to further our understanding of magma system and crustal evolution. We propose that titanite, which is a common accessory in metaluminous and weakly peraluminous granites, can be used as a barometer if it crystallized in magmatic, near-solidus conditions and in equilibrium with amphibole, plagioclase, K-feldspar, quartz, biotite, and magnetite ± ilmenite. Titanite Al_2O_3 increases with pressure (P) according to: P (in MPa) = 101.66 × Al_2O_3 in titanite (in wt%) + 59.013 (R^2 = 0.83) with estimated uncertainties of ~±60 to ~±100 MPa for crystallization between ~150 and 400 MPa. We highlight that the current calibration dataset is limited, and that systematic experimental studies are needed to rigorously quantify the relation. The most important use of this empirical barometer will be for rocks in which amphibole is present but significantly altered, or in combination with amphibole barometry, as titanite can be easily dated by LA-ICP-MS.

1. Introduction

Estimates on crystallization pressure for igneous systems provide key constraints on where in the crust magma ponding takes place in a range of geodynamic settings (Anderson et al., 2008; Blundy and Cashman, 2008; Scaillet et al., 2016). Constraints on crystallization pressure for granitic magma systems are based on phase-equilibrium experiments, pressure-sensitive mineral assemblages and their composition, and rarely on CO_2 and H_2O contents of fluid or melt inclusion studies, as fluid and crystallized melt inclusion compositions typically get reset during slow cooling (e.g., Anderson et al., 2008; Bartoli et al., 2014; Clemens and Wall, 1981; Dall'Agnol et al., 1999; Harlov et al., 2013; Mutch et al., 2016; Scaillet et al., 1995, 2016). Hornblende is the most commonly employed mineral barometer for silicic plutonic systems, for which the Al content increases with pressure, but also with other intensive parameters, including temperature, oxygen fugacity, and magma/melt/fluid composition (Anderson and Smith, 1995; Erdmann et al., 2014; Hammarstrom and Zen, 1986; Holland and Blundy, 1994; Hollister et al., 1987; Johnson and Rutherford, 1989; Mutch et al., 2016; Putirka, 2016; Schmidt, 1992; Zhang et al., 2017). Hornblende is thus a useful barometer, if the variation in intensive parameters other than pressure is limited or well-constrained, as is typically the case for amphibole crystallized from granitic magmas in near-solidus conditions and in equilibrium with a multiply saturated phase assemblage

* Corresponding author. State Key Laboratory for Mineral Deposit Research, School of Earth Sciences and Engineering, Nanjing University, China.
E-mail address: saskia.erdmann@cnrs-orleans.fr (S. Erdmann).

https://doi.org/10.1016/j.crte.2019.09.002

(e.g., Anderson and Smith, 1995; Hammarstrom and Zen, 1986, 1992; Mutch et al., 2016).

Like amphibole, titanite is known to incorporate increasing amounts of Al with increasing pressure (Markl and Piazolo, 1999; Oberti et al., 1991; Smith, 1981; Tropper et al., 2002). The titanite Al content, however, also varies with intensive parameters other than pressure, mostly with magma, melt, rock, and/or temperature (e.g., Bernau and Franz, 1987; Carswell et al., 1996; Enami et al., 1993; Markl and Piazolo, 1999). The thermobarometric potential of titanite has been previously considered for subsystems (Enami et al., 1993), but it has been questioned where a large range of whole-rock/system compositions was considered (Markl and Piazolo, 1999). We test here if titanite crystallized from granites in magmatic near-solidus conditions in rocks with the equilibrium assemblage of titanite–amphibole–biotite–quartz–plagioclase–K-feldspar–magnetite ± ilmenite may be a useful barometer in a similar fashion as existing Al-in-hornblende solidus barometers, i.e. in cases in which variation in intensive parameters other than pressure (e.g., temperature, composition) was limited during its crystallization. Titanite could provide barometric constraints in addition to amphibole and for rocks in which amphibole is significantly altered. Titanite, moreover, has the advantage that it can be easily and accurately dated by LA–ICP–MS (Storey et al., 2006; Sun et al., 2012), and that it has been developed as a metallogenetic indicator (Pan et al., 2018; Xie et al., 2010).

2. Data and methods

We use a combination of new and published compositional data and petrographic observations for titanite, amphibole, and plagioclase from nine granitic intrusions as summarized in Supplementary Tables 1 and 2. We highlight that most granites comprise titanite, which is interpreted to have crystallized from sub-solidus fluids (the so-called "hydrothermal titanite") in addition to titanite crystallized in magmatic conditions. The hydrothermally crystallized titanite typically forms irregular rims on magmatic crystals or unzoned, interstitial crystals (Fig. 1). The hydrothermally crystallized zones are characterized by high-F and/or Cl and low Fe_2O_3 and Zr contents (e.g., see also Aleinikoff et al., 2002; Broska et al., 2007; Che et al., 2013; Xie et al., 2010), which are easily identified in back-scattered electron imaging mode and/or through electron microprobe analysis. The composition of any hydrothermal titanite has been excluded from our dataset, and such compositions also have to be identified and excluded in studies considering the Al-in-titanite barometric relation that we propose.

We first use amphibole and ±plagioclase compositions to independently estimate the crystallization temperature and pressure for the nine considered granite intrusions. We then use the estimated amphibole crystallization pressures to evaluate titanite's Al compositional variation as a function of the magmatic crystallization pressure. We have taken this approach as accurate compositional data for titanite experimentally crystallized in granitic systems in magmatic near-solidus conditions are not available to date. The main reason for this is that titanite crystallized in such conditions is typically $\leq$2–5 μm in maximum dimension, resulting in contaminated compositional analyses.

We have determined titanite, amphibole, and plagioclase compositions for crystals from the Shipi, the Guposhan, and the Qiatianling plutons of southeast China, and for two unnamed intrusions on Melville Peninsula, Nunavut, northern Canada. Published data for the Qitianling and the Guposhan intrusions from Xie et al. (2010) and Wang et al. (2013) are also considered. Published data that we have used in addition are for titanite, amphibole, and plagioclase from the Mount Princeton batholith, Colorado, United States (data from Ackerson, 2010; Toulmin and Hammarstrom, 1990), from the Tuolumne batholith, California, Unites States (Half Dome and Cathedral Peak units; data from Solgadi, 2010), from the Soultz-sous-Forêts pluton, Alsace, France (data from Stussi et al., 2002), and from the Ävrö granite, Äspö, Sweden (data from Morad et al., 2009). These four intrusions were considered to supplement our data, as their geology and petrology are described in sufficient detail, as we were able to find the compositional data that are necessary for our evaluation, and as they have crystallized at pressures where our data are limited. We did not consider granitic systems, if we were uncertain if amphibole and/or titanite were in equilibrium (e.g., Mesquita et al., 2018), or if we suspected partial hydrothermal alteration of magmatic crystals (e.g., Fe-poor and F-rich compositions reported by Enami et al., 1993). We have classified whole-rock compositions of the considered samples according to Fe* ($Fe^{tot}/[FeO^{tot} + MgO]$), molar $Na_2O + K_2O–CaO$, and ASI (molar Al/[Ca−1.67P + Na + K]), following Frost et al. (2001) (Fig. 2). The mineral abbreviations used are those of Whitney and Evans (2010). Reported titanite compositions are compositions of magmatic crystal cores. In our samples and where they have been described in detail, titanite typically shows small-scale oscillatory zoning and limited core-rim zoning. Following others, we show Fe as Fe_2O_3 (total), given that most Fe in titanite is present as Fe^{3+} (Enami et al., 1993; King et al., 2013; Oberti et al., 1991). Amphibole crystals in our samples, and where they have been described in detail, are also mostly unzoned (Fig. 1a, b), except for some crystals that show evidence of alteration, and we have therefore focussed on presenting magmatic core compositions in the figures and tables.

We have calculated amphibole stoichiometry based on 23 oxygens for the thermometric and barometric calculations as required by the different calibrations. The amphibole crystallization pressure was determined using the Al-in-hornblende barometer of Mutch et al. (2016), which is applicable to granite bulk compositions (sensu lato) from which amphibole has crystallized between ~80 and 1000 MPa. The calibration has the largest database of all currently available amphibole barometers for granitic systems, including data from previous calibrations. It has an estimated uncertainty of ±16%, using the hornblende Al (total) content as the only input parameter, but also requires amphibole crystallization at 725 ± 75 °C, and equilibrium with plagioclase (An15-80)–biotite–quartz–K-feldspar–ilmenite/titanite–magnetite and a H_2O-rich fluid (X_{H2O} > ~0.9). All our considered samples have the

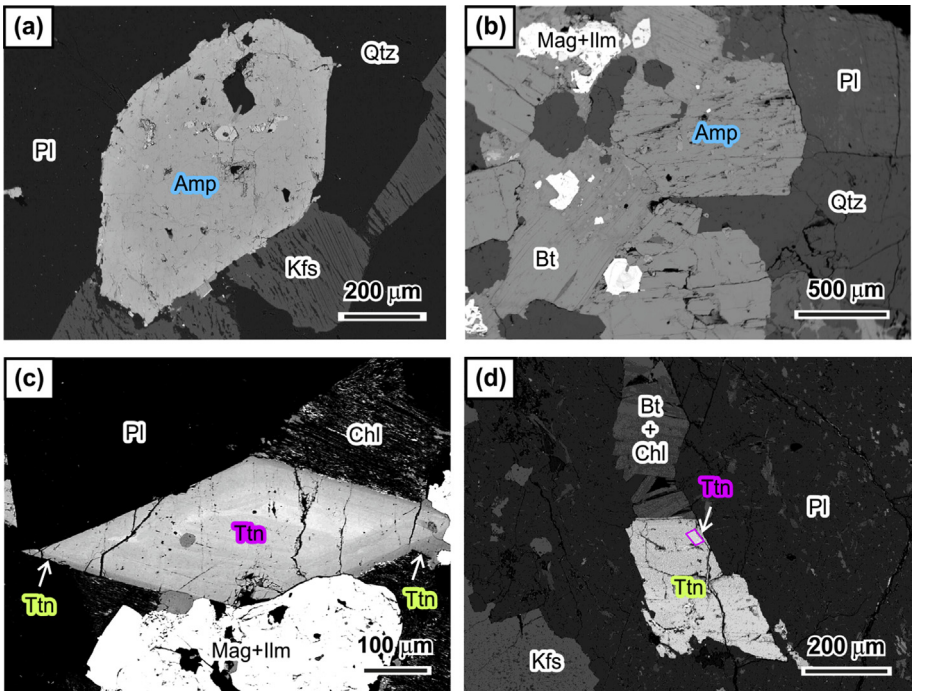

Fig. 1. Backscattered electron (BSE) images showing typical (a,b) magmatic amphibole, and (c,d) magmatic and hydrothermal titanite crystals and crystal zones. (a) Euhedral, largely unzoned single amphibole crystal, and (b) euhedral-subhedral cluster of largely unzoned amphibole and biotite crystals in the Qitianling granites. (c) Typical euhedral, oscillatory-zoned magmatic titanite crystal (pink label) from the Shipi intrusion with thin, <50 µm wide, irregular rim of hydrothermal titanite (green labels). The hydrothermally crystallized rim, which is notably absent in contact with magmatic plagioclase and magnetite, is characterized by a relatively dark BSE response. (b) Interstitial, largely unzoned hydrothermal titanite (green label) from the Guposhan intrusion with an apparent inclusion of a euhedral, magmatic titanite crystal (pink label and outline), which is likely the tip of a larger crystal. Amp = amphibole; Ttn = titanite; Pl = plagioclase; Kfs = K-feldspar; Bt = biotite; Mag = magnetite; Ilm = ilmenite; Chl = chlorite.

appropriate mineral assemblage for applying the barometer. The presence of amphibole records that melt H_2O contents were >4 wt% at least in near-solidus conditions (e.g., Dall'Agnol et al., 1999; Huang et al., 2019). That X_{H_2O} of the systems was >0.9 is possible (probable), as we have no evidence of abundant CO_2 in the studied systems, but even a relatively low X_{H_2O} of ~0.75 has no effect on the calculated pressure beyond the uncertainty of the method (cf. Mutch et al., 2016).

Amphibole crystallization temperatures were calculated using the amphibole equation 5 and equation 6 thermometers of Putirka (2016) and the amphibole–plagioclase thermometer of Holland and Blundy (1994; equation A for quartz-bearing equilibrium assemblages). The two applied thermometers of Putirka (2016) have been calibrated for igneous calcic amphibole. The equation 5 thermometer requires amphibole Si, Ti, Fe, and Na composition as input; the equation 6 thermometer also requires a pressure estimate, for which we have used the calculated amphibole pressures. The range of application is not explicitly defined for the thermometers, while both calibrations are inferred to have standard errors of ~±50 °C. The Holland and Blundy (1994) amphibole–plagioclase equation A thermometer was formulated for estimating crystallization temperatures between 400 and 900 °C, for a wide range of amphibole and whole-rock compositions, and at an estimated uncertainty of ±40 °C. Input parameters are amphibole Si, Al, Fe, Mg, Ca, Na, and K composition, plagioclase An content, and pressure, for which we have used the values calculated using the Mutch et al. (2016) calibration. The thermometer requires Ca > 1.5 apfu, Si = 6.0–7.7 apfu, Al^{VI} < 1.8 apfu, Na > 0.02 apfu, and plagioclase An < 90. Anderson and Smith (1995) suggest that the thermometer should not be applied to amphibole with calculated $Fe^{3+}/(Fe^{3+}+Fe^{2+}) \lesssim 0.20–0.25$, estimated on the basis of 23 oxygens. We stress that several of our amphibole compositions have $Fe^{3+}/(Fe^{3+}+Fe^{2+}) < 0.20$ (i.e. all amphibole from the studied ferroan granites), for which we have nevertheless calculated crystallization temperatures, but only for a complete and critical discussion. We also note that the calculated Fe^{3+} and Fe^{2+} contents for amphibole vary significantly depending on the stoichiometric model considered and on the abundance of unquantified species (Hawthorne et al., 2012; Schumacher, 1997), and that the calculated values should therefore not be quantitatively interpreted.

3. Geological context

The considered granites are from locations in China, Canada, France, Sweden, and the United States. The Tertiary Mount Princeton batholith (United States, Colorado) is exposed over ~25 km × 35 km, forming a shallow, subcaldera intrusion at the northern end of the Southern Rocky Mountain volcanic field (Lipman, 2007; Toulmin and Hammarstrom, 1990). The Late Cretaceous Tuolumne

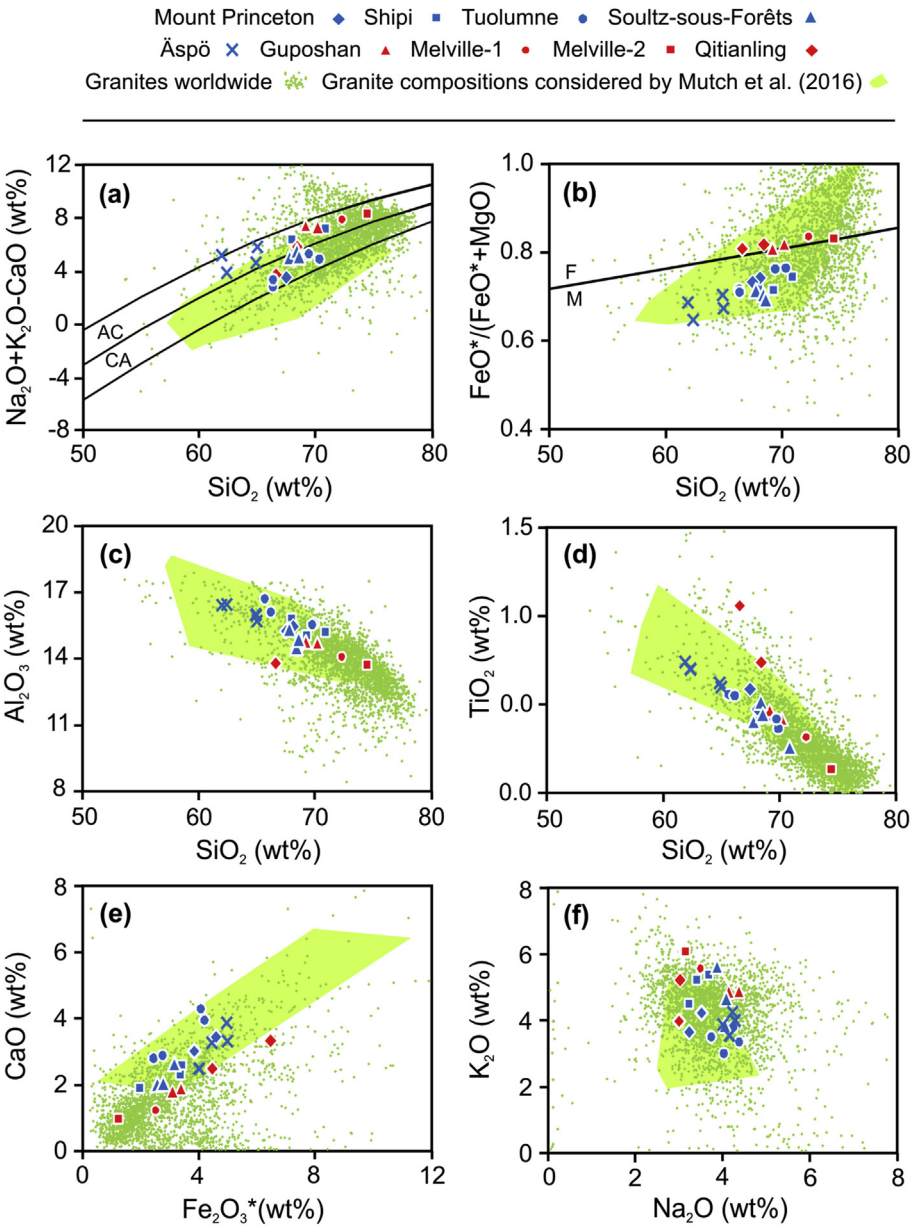

Fig. 2. Whole-rock composition of samples from which titanite and amphibole compositions were considered (red and blue symbols, see legend for details), granite (sensu lato) compositions from the GeoRoc database (green symbols), and the range of granite compositions from which amphibole has been used for the calibration of the Mutch et al. (2016) Al-in-hornblende barometer (green field). (a,b) Classification diagrams of Frost et al. (2001) where AC = alkali-calcic, CA = calc-alkalic, F = ferroan, and M = magnesian. All compositions were re-normalized to 100 wt% anhydrous. * Total iron calculated as FeO or Fe_2O_3, respectively. Data for Mount Princeton are from Toulmin and Hammarstrom (1990), for Shipi from this study, for Tuolumne from Solgadi (2010), for Soultz-sous-Forêts from Stussi et al. (2002), for Äspö from Drake et al. (2006), for Guposhan from Wang et al., 2014, for Melville from Erdmann et al. (2013), and for Qitianling from Huang et al. (2019).

batholith (California, United States) is exposed over ~30 km × 50 km, emplaced into a basement of metasedimentary and granitoid rocks (Bateman, 1992). The Mount Princeton and Tuolumne granites formed from fractionated, crustally-contaminated yet mantle-derived magmas (Bateman, 1992; Johnson et al., 1990). The Paleoproterozoic Äspö granites are exposed in a suite of diorites and granites in southeastern Sweden (Drake et al., 2006; Morad et al., 2009). The Carboniferous Soultz-sous-Forêts monzogranites, which mostly have crustal sources but a mantle-derived component, were emplaced into granitic basement during the Varsican orogeny (Stussi et al., 2002). The Shipi pluton (China, Fujian) comprises Jurassic (hornblende-free) granites and a small (~10 km × 20 km) stock of Cretaceous, hornblende-bearing granites, which we have characterized. The granites primarily represent crustally-derived melts, but they also comprise a mantle-derived melt component (Wang et al., 2016). The Jurassic

Qitianling and Guposhan plutons crop out over ~50 km × 50 km in the Nanling Range of southeast China, representing crustal melts with limited mantle input (Shu et al., 2011; Wang et al., 2014; Zhao et al., 2005). The Paleoproterozoic Melville granites (Canada, Nunavut) form small-scale intrusions exposed over < 5 km^2 that are part of a ~100–300-km-wide granite belt. They represent crustal melts with no mantle input (Erdmann et al., 2013).

4. Results and discussion

4.1. Whole-rock compositions and petrography

The considered granites have compositions that compare to those of granites worldwide (Fig. 2). They are (1) magnesian, calc-alkalic to alkali-calcic, and metaluminous to peraluminous monzogranites; and (2) ferroan, calc-alkalic to alkali-calcic, and metaluminous to peraluminous monzogranites (Fig. 2a, b). The SiO_2 content of the magnesian and ferroan granites overlaps (Fig. 2a–d), while the magnesian ones tend to lower SiO_2 and TiO_2, yet to higher MgO, Al_2O_3 and CaO (Fig. 2b–e) than the ferroan granites. Most of the considered granite samples match the compositions of granites from which amphibole compositions have been used to calibrate the Al-in-hornblende barometer of Mutch et al. (2016), with the exception of the most TiO_2-rich and the some relatively CaO-poor ferroan granite samples (Fig. 2d, e).

All granites have the characteristic assemblage amphibole–titanite–biotite–plagioclase–K-feldspar–quartz–magnetite ± ilmenite (our data; Erdmann et al., 2013; Morad et al., 2009; Solgadi, 2010; Toulmin and Hammarstrom, 1990; Wang et al., 2014, Supplementary Table 1), where amphibole and titanite form subhedral to euhedral phenocrysts (Fig. 1). Amphibole is largely unzoned, showing compositional core plateau zones (Fig. 1a, b), while crystals locally show patchy zoning and low-temperature alteration to chlorite (our observations; Solgadi, 2010; Stussi et al., 2002; Toulmin and Hammarstrom, 1990). Amphibole replacement by biotite or titanite, in contrast, is not observed (Fig. 1a, b) or described in the literature examples. Some titanite crystals show sector zoning in their cores, while most crystals are largely unzoned (our observations; Ackerson, 2010), except for fine-scale oscillatory zoning (Fig. 1c). Largely unzoned, hydrothermally crystallized titanite is variably present (Fig. 1c, d), but was excluded from our analyses and considerations.

4.2. Amphibole composition and crystallization conditions

All amphibole from the considered samples is calcic, with magnesiohornblende composition in the magnesian granites and with ferroedenite to hastingsite composition in the ferroan granites (Supplementary Table 1; Fig. 3, following the classifications of Leake et al. (1997) and Frost et al. (2001)). Amphibole from the magnesian granites has lower Al_2O_3, TiO_2, and ±Na_2O (Fig. 3a–c) yet higher SiO_2 and X_{Mg} (Fig. 3d) than amphibole from the ferroan granites. The higher X_{Mg} and lower TiO_2 of amphibole from the magnesian granites as compared to the ferroan granites mirror the whole-rock compositional differences (Figs. 3b, d versus 2b, d), while the low Al_2O_3 content of amphibole contrasts with the high Al_2O_3 contents of the magnesian whole rocks (Figs. 3a versus 2c). The calculated $Fe^{3+}/(Fe^{3+} + Fe^{2+})$ values are higher for amphibole from the magnesian granites ($\gtrsim$ 0.20) than for amphibole from the ferroan granites (<0.19; Supplementary Table 1; Fig. 3f), which attests to more oxidizing conditions in the magnesian magma systems.

Crystallization temperatures calculated using the Putirka (2016) equations 5 and 6 thermometers range between ~715 and ~800 °C for amphibole from both granite types, and they are thus significantly above the H_2O-rich granite solidus (Fig. 3g; Supplementary Table 1). We interpret them as significant overestimates (1) because textures (subhedral-euhedral morphology) record that amphibole was stable at the solidus (i.e. crystals were not partially replaced by other magmatic phases such as biotite or titanite) and (2) because the largely unzoned character of the amphibole crystals indicates crystallization and/or equilibration at the solidus, and not over a large temperature range (e.g., from near-liquidus to near-solidus temperatures). The calculated temperatures are thus mostly above the estimated standard errors of the method (~±50 °C) but within maximum errors of ~150 °C (cf. Fig. 5g, h of Putirka, 2016) of haplogranite solidus temperatures. We stress that our choice of input pressures (calculated using the Mutch et al. (2016) calibration) has no significant effect on the calculated crystallization temperatures, i.e. a change by ±500 MPa results in a <±10 °C variation of the calculated temperatures. Considering the range of Putirka's calibration data (where > 95% of the data are for amphibole crystallized at 750–1100 °C), we suggest that the thermometers should not be used for amphibole crystallized from granitic magmas in near-solidus conditions. The amphibole–plagioclase crystallization temperatures calculated using the Holland and Blundy (1994) equation A thermometer for quartz-bearing assemblages are also high (~700–890 °C) for amphibole from the ferroan granites with calculated $Fe^{3+}/(Fe^{3+} + Fe^{2+})$ of 0.06–0.19 (on average ~0.07–0.13; Fig. 3h; Supplementary Table 1). The input pressure decreases the calculated temperatures (by ~15 °C for 100 MPa), and thus cannot account for the differences in calculated crystallization temperatures of ~700–890 and ~630–20 °C for the ferroan and magnesian systems with inferred crystallization pressures of ~260–430 and ~130–240 MPa, respectively (Fig. 3g, h; Supplementary Table 1). As alluded to by Anderson and Smith (1995), temperatures calculated for the Fe^{3+}-poor amphibole crystals from the ferroan granites, which have crystallized in relatively reducing conditions, should not be considered for temperature estimates using the Holland and Blundy (1994) calibration (Fig. 3f, h) (for which the amphibole Na–K content is used in the calculation, which is dependent on temperature, but also strongly on the amount of Fe^{3+} substitution and coupled vacancies on the A- and B-sites). The amphibole–plagioclase temperatures calculated for the magnesian granites with calculated amphibole $Fe^{3+}/(Fe^{3+}+Fe^{2+})$ of ~0.20–0.30 or higher, in contrast, are close to the haplogranite solidus, which we consider as robust and realistic estimates (Fig. 3h; Supplementary Table 1). Independent estimates further suggest that the

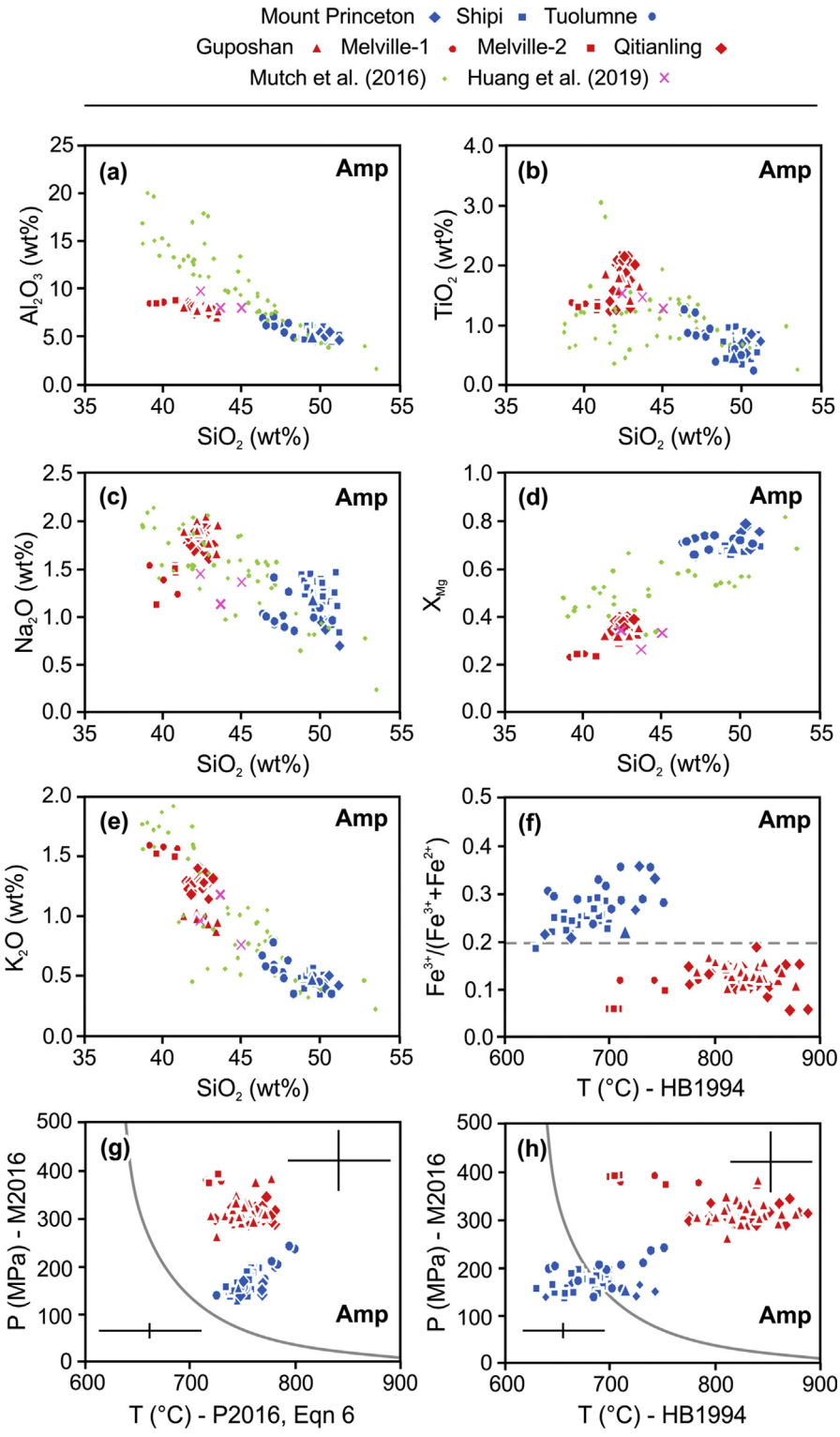

Fig. 3. Amphibole compositions (a–e) and calculated crystallization conditions (f–h). Data from the Mutch et al. (2016) amphibole barometer calibration dataset and from Huang et al. (2019) for amphibole crystallized in 300 MPa experiments and at ≤750 °C are shown for comparison. T = temperature; P = pressure; HB1994 = Holland and Blundy (1994); M2016 = Mutch et al. (2016); and P2016 = Putirka (2016). (f) Amphibole with calculated $Fe^{3+}/(Fe^{3+}+Fe^{2+})$ <0.20–0.25 (below the grey dashed line) should not be employed for estimating the crystallization temperature using the Holland and Blundy (1994) thermometers (cf. Anderson and Smith, 1995). (g,h) Solid grey lines show the approximate location of the H_2O-saturated haplogranite solidus of Holtz et al. (2001); the black crosses highlight the inferred uncertainties of the estimates at low- and high-pressure (±40–50 °C and ±16% for pressure). We note that the Äspö amphibole's

granites and amphibole of the magnesian and ferroan intrusions crystallized at comparable temperatures, i.e. at ≲ 700 and ≥650 °C (Supplementary Table 1). The thermometers of Putirka (2016) adequately capture this relation (i.e. comparable crystallization temperatures, while they overestimate crystallization temperatures), likely because they consider the amphibole Ti and Fe contents in addition to the Si and Na contents, which relate to fO_2 variation.

The amphibole crystallization pressures calculated using the Mutch et al. (2016) barometer indicate that the magnesian granites formed at lower pressures (~130–240 MPa) than the ferroan granites (~260–390 MPa), where data are clustered at ~150–200 and at ~300–390 MPa (Fig. 3g, h). The inferred near-solidus crystallization of the equilibrium assemblage amphibole–plagioclase–K-feldspar–quartz–biotite–titanite–magnetite ± ilmenite makes the barometer applicable, ruling out that the variation in the Al content of the amphibole and thus the calculated pressure variation is an artefact of highly variable crystallization temperature. Differences in the composition of the system Al_2O_3/SiO_2 equally cannot account for the variable amphibole Al_2O_3 and thus the calculated pressure difference, as amphibole from the relatively Al_2O_3-rich, magnesian granites is Al-poor compared to amphibole from the Al_2O_3-poor, ferroan granites (Fig. 2c). That amphibole from the ferroan granites partly differs in composition from the ones used in the Mutch et al. (2016) barometric calibration (Fig. 3a–d) could be problematic for our pressure estimates. We note, however, that the Al_2O_3 content of amphibole from the ferroan granites (e.g., phase equilibrium experiments of Huang et al., 2019) and the Al_2O_3 content of amphibole from the calibration experiments of Mutch et al. (2016) are equivalent (e.g., ~8.9 versus ~9.5 wt%), which is important as pressures are calculated using the total Al content. Variation in oxygen fugacity, which we infer for the ferroan granites (relatively reducing) and the magnesian granites (relatively oxidizing) affects amphibole's X_{Mg} and TiO_2 composition, but not its Al_2O_3 content (e.g., data compilation in Erdmann et al., 2014). We therefore consider the variation in the amphibole Al content to be largely a primary record of pressure and suggest that the differences in pressure determined for the magnesian granites (~150–230 MPa) and the ferroan granites (~300–390 MPa) are robust and realistic estimates (Supplementary Table 1). The calculated amphibole crystallization pressures are also consistent with independent estimates for the Melville-1, the Mount Princeton, and the Qitianling intrusions (Supplementary Table 1).

4.3. Titanite composition and crystallization conditions

Titanite, like amphibole, shows considerable compositional variation in the considered intrusions (Fig. 4; Supplementary Table 2). Titanite crystals from the magnesian granites have low Al_2O_3 and high TiO_2 contents compared to the crystals from the ferroan granites (Fig. 4a), where Al_2O_3 and TiO_2 show a negative correlation. Al_2O_3 and Fe_2O_3 (total) contents are positively correlated for titanite from individual systems, but not for the entire dataset (Fig. 4b). SiO_2 and Fe_2O_3 (total) concentrations closely compare in titanite from all granites, but tend to be slightly higher for titanite from the ferroan granites (Fig. 4b, c).

Titanite crystals from our dataset are characterized by limited core-rim zoning. Their CaO and TiO_2 contents show oscillatory zoning and a weak increase from core to rim (Fig. 5a). CaO and TiO_2 correlate negatively with the analytical totals of the microprobe analyses, indicating that they are variably substituted by undetected elements (mostly REEs and HFSEs; King et al., 2013). Fe_2O_3 (total) and F are negatively correlated (Fig. 5b), showing minor compositional variation. Core-rim and oscillatory zoning are taken to record limited temperature and compositional evolution and kinetics of crystallization. Al_2O_3 shows no significant zoning (Fig. 5a, b), highlighting that its concentration could have been largely controlled by the crystallization pressure.

For titanite core compositions from the nine studied intrusions, we note an increase of $Al_2O_3 \pm Fe_2O_3$ (total) at the expense of TiO_2 (Fig. 4a, d; Supplementary Table 2). The composition of the melts that were in equilibrium with titanite is unknown, but the magnesian and the ferroan whole rocks have overlapping Al_2O_3/TiO_2 and $Al_2O_3+Fe_2O_3$ (total)/TiO_2 (Fig. 2c, d), while titanite from the magnesian granites has lower Al_2O_3/TiO_2 ratios than crystals from the ferroan granites (Fig. 4a), and we thus suggest that magma/melt compositional variation did not primarily control the variable Al_2O_3 compositions of titanite. Titanite $Al_2O_3+Fe_2O_3$ (total)/TiO_2 is known to increase with decreasing temperature (Enami et al., 1993), and the higher $Al_2O_3+Fe_2O_3$ content of titanite in the ferroan granites could thus indicate crystallization at lower temperature. We infer, however, that amphibole and titanite from both granite types have crystallized in near-solidus conditions at < 700 and ≥650 °C, while we note that an increase of TiO_2 over $Al_2O_3+Fe_2O_3$ from core to rim in crystals (e.g., Fig. 5) likely records crystallization during minor cooling (cf. Enami et al., 1993). Oxygen fugacity has been proposed as a possible control on titanite Fe_2O_3 (total) and Al_2O_3 composition, where it was suggested that Fe_2O_3 (total) increases at the expense of Al_2O_3 in increasingly oxidizing conditions (Pan et al., 2018), while no direct evidence of such substitution (e.g., through measurement of Fe^{2+}/Fe^{3+} concentrations) has been provided. We have no direct constraints on the Fe^{2+}/Fe^{3+} compositions of our titanite crystals, but we observe a weak positive (not a negative) correlation between the titanite Al_2O_3 and Fe_2O_3 (total) contents, at least for individual systems (Fig. 4b). We further highlight that the titanite Fe_2O_3 (total) contents of the crystals largely overlap, while the Al_2O_3 contents do not, which argues against fO_2 variation as a primary

composition is not shown, as Morad et al. (2009) reported only major element and some minor element compositions for amphibole (in apfu), which we have used for our pressure calculations (Supplementary Table 2).

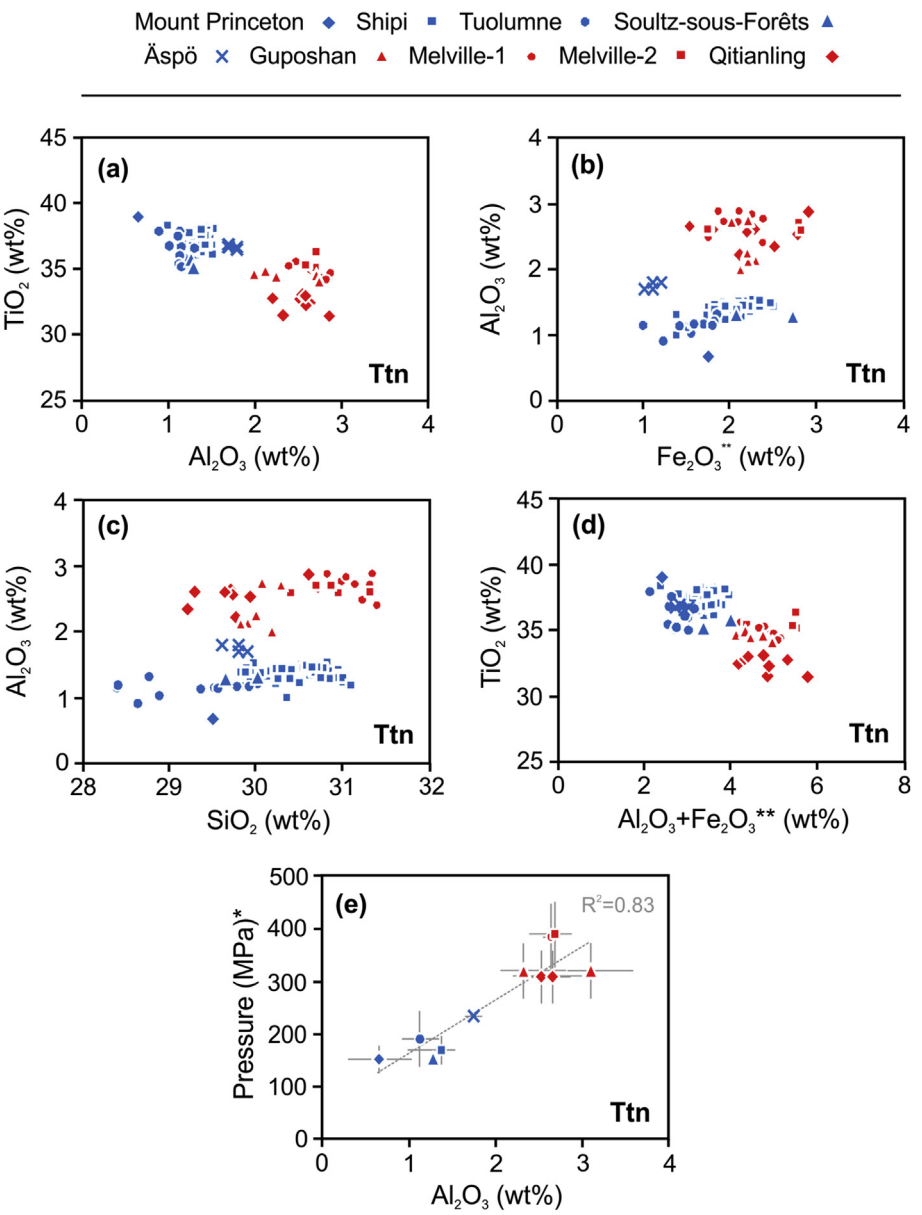

Fig. 4. Titanite compositions (a–d) and calculated crystallization conditions (e). *Average pressure determined using amphibole composition and the calibration of Mutch et al. (2016); values are reported in Supplementary Tables 1 and 2. ** Total iron reported as Fe_2O_3. Titanite Al_2O_3 positively correlates with calculated amphibole pressure. Systematic, experimental data are needed to rigorously constrain the relation and its uncertainties. The grey, vertical bars indicate the ±16% uncertainty for the calculated hornblende crystallization pressures; the grey, horizontal bars indicate the detected Al_2O_3 compositional variation.

compositional control on titanite Al_2O_3. As for amphibole, we therefore posit that the Al_2O_3 content of the titanite crystals, which formed in magmatic, near-solidus conditions and in equilibrium with the assemblage of amphibole, plagioclase, K-feldspar, quartz, biotite, and magnetite ± ilmenite, is largely controlled by the crystallization pressure, which is in agreement with the qualitative evaluation of Enami et al. (1993).

Titanite Al ± Fe substitute for Ti (Fig. 4a, d; Supplementary Table 2; cf. Enami et al., 1993), while other elements also substitute for Ti (e.g., King et al., 2013). Relating the titanite Al_2O_3 content and the crystallization pressure estimated using the amphibole compositions, a linear fit to the data for the nine intrusions yields:

$$P\,(\mathrm{MPa}) = 101.66 \times (\mathrm{Al_2O_3\ Ttn\ wt\%}) + 59.013\ (R^2 = 0.83)$$

We suggest that the proposed barometric equation can be used to distinguish between titanite formed at relatively low pressure (e.g., at ≤200 MPa) and titanite formed at relatively high pressure (e.g., at ~300–400 MPa). We caution that the barometer may not

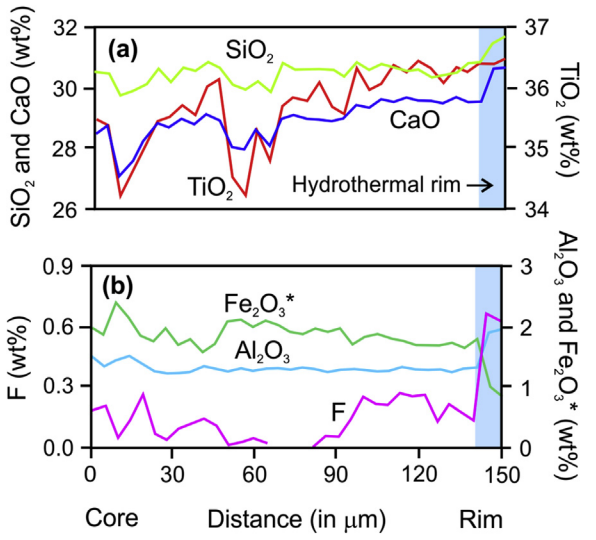

Fig. 5. Characteristic core-rim compositional profiles for titanite (example from the Shipi intrusion). * Total iron reported as Fe_2O_3. Note that core-rim and small-scale oscillatory zoning likely record near-solidus cooling, melt compositional variation, and crystallization kinetics.

perform at higher or at lower pressure (i.e. at > 500 and ≤100 MPa), where the inferred linear relationship may not apply (e.g., as inferred for amphibole by Mutch et al., 2016), and we highlight that most calibration data cluster between ~150 and 200 and ~300 and 390 MPa (Fig. 4e). All calculated titanite pressures are within ±54 and on average within ±30 MPa of the calculated amphibole pressures (Supplementary Table 2). Average uncertainties appear thus to be ~±60 to ~±100 MPa for calculated pressures between ~150 and 400 MPa (considering our average error plus an estimated 16% uncertainty of the Mutch et al. (2016) calibration). We stress, however, that the limited dataset does not allow us to rigorously constrain uncertainty, and we thus recommend that the calibration and its uncertainty are critically evaluated. Additional, high-quality data are needed to rigorously constrain titanite's compositional variation as a function of pressure, while characterizing and correcting for the effect of variation in other intensive parameters (e.g., limited near-solidus temperature variation).

We have tested the proposed equation for titanite compositions from Cu–Au and W–Mo mineralized, Late Triassic–Early Jurassic porphyries from Mount Milligan and Boss Mountain in British Columbia, Canada. Magmatic titanite from the Mount Milligan and Boss Mountain porphyries has on average ~0.97 wt% Al_2O_3 (Celis, 2010; Che et al., 2013), calculating crystallization pressures of ~158 MPa, (Supplementary Table 2). Tight, independent pressure estimates do not exist for the porphyries, but (1) stratigraphic constraints suggest crystallization pressures of >90 MPa for the Boss Mountain porphyries (del Real et al., 2017), while (2) amphibole crystallization pressures of spatiotemporally associated ore-bearing porphyries indicate crystallization at ~110–200 ± 40 MPa (Zhu et al., 2018), thus bracketing our titanite pressure estimates.

5. Conclusions

We propose that the Al content of titanite crystallized from granitic magmas (sensu lato) in magmatic near-solidus conditions and in equilibrium with amphibole–plagioclase–K-feldspar–quartz–biotite–magnetite ± ilmenite records pressure variation in a similar fashion as the Al content of amphibole. We propose a preliminary empirical barometer with pressure (P in MPa) = 101.66 × (Al_2O_3 Ttn wt%) + 59.013 (R^2 = 0.83), based on amphibole barometric constraints. Systematic, experimental data collection, and critical application are needed to achieve the accuracy of current Al-in-hornblende barometers and to define titanite's compositional variation as a function of pressure independently of that of amphibole, while constraining the effect of minor, near-solidus temperature and compositional variation or the variation of other intensive parameters on titanite Al_2O_3 content.

Funding

S.E acknowledges a post-doctoral scholarship from Nanjing University and support for all analytical work through National Science Foundation of China awards to Prof. Rucheng Wang (NSFC grants 41230315 and 41611130111).

Appendix A. Supplementary data

Supplementary data related to this article can be found at https://doi.org/10.1016/j.crte.2019.09.002.

References

Ackerson, M.R., 2010. Trace Element Partitioning between Titanite and Groundmass in Silicic Volcanic Systems. M.Sc. Thesis. University of North Carolina at Chapel Hill, NC, USA, pp. 1–76.
Aleinikoff, J.N., Wintsch, R.P., Fanning, C.M., Dorais, M.J., 2002. U-Pb geochronology of zircon and polygenetic titanite from the Glastonbury Complex, Connecticut, USA: an integrated SEM, EMPA, TIMS, and SHRIMP study. Chem. Geol. 188 (1–2), 125–147.
Anderson, J.L., Smith, D.R., 1995. The effects of temperature and f_{O_2} on the Al-in-hornblende barometer. Am. Mineral. 80 (5–6), 549–559.
Anderson, J.L., Barth, A.P., Wooden, J.L., Mazdab, F., 2008. Thermometers and thermobarometers in granitic systems. Rev. Mineral. Geochem. 69, 121–142.
Bartoli, O., Cesare, B., Remusat, L., Acosta-Vigil, A., Poli, S., 2014. The H_2O content of granite embryos. Earth Planet. Sci. Lett. 395, 281–290.
Bateman, P.C., 1992. Plutonism in the Central Part of Sierra Nevada Batholith, California. USGS Prof. Pap. 1483, pp. 1–186.
Bernau, R., Franz, G., 1987. Crystal chemistry and genesis of Nb-, V-, and Al-rich metamorphic titanite from Egypt and Greece. Can. Mineral. 25, 695–705.
Blundy, J., Cashman, K., 2008. Petrologic reconstruction of magmatic system variables and processes. Rev. Mineral. Geochem. 69 (1), 179–239.
Broska, I., Harlov, D., Tropper, P., Siman, P., 2007. Formation of magmatic titanite and titanite–ilmenite phase relations during alteration in the Tribeč Mountains, Western Carpathians, Slovakia. Lithos 95 (1–2), 58–71.
Carswell, D.A., Wilson, R.N., Zhai, M., 1996. Ultra-high pressure aluminous titanites in carbonate-bearing eclogites at Ahuanghe in Dabieshan, central China. Miner. Mag. 60, 461–471.
Celis, A., 2010. Titanite as an Indicator Mineral for Alkalic Porphyry Cu–Au Deposits in South-Central British Columbia. M.Sc Thesis. University of British Columbia, Canada, pp. 1–266.
Che, X.D., Linnen, R.L., Wang, R.C., Groat, L.A., Brand, A.A., 2013. Distribution of trace and rare earth elements in titanite from tungsten and

molybdenum deposits in Yukon and British Columbia, Canada. Can. Mineral. 51 (3), 415–438.
Clemens, J., Wall, V.J., 1981. Origin and crystallization of some peraluminous (S-type) granitic magmas. Can. Mineral. 19 (1), 111–131.
Dall'Agnol, R., Scaillet, B., Pichavant, M., 1999. An experimental study of a lower Proterozoic A-type granite from the Eastern Amazonian Craton, Brazil. J. Petrol. 40 (11), 1673–1698.
del Real, I., Bouzari, F., Rainbow, A., Bissig, T., Blackwell, J., Sherlock, R., Thompson, J.F.H., Hart, C.J.R., 2017. Spatially and temporally associated porphyry deposits with distinct Cu/Au/Mo ratios, Woodjam District, Central British Columbia. Econ. Geol. 112 (7), 1673–1717.
Drake, H., Sandström, B., Tullborg, E.-L., 2006. Svensk Kärnbränslehantering AB Mineralogy and geochemistry of rocks and fracture fillings from Forsmark and Oskarshamn: compilation of data for SRCan. Swedish Nucl. Fuel Waste Manag. Rep. R- 06–109, 101.
Enami, M., Suzuki, K., Liou, J.G., Bird, D.K., 1993. Al–Fe^{3+} and F–OH substitutions in titanite and constraints on their *P–T* dependence. Eur. J. Mineral. 5 (2), 219–231.
Erdmann, S., Wodicka, N., Jackson, S.E., Corrigan, D., 2013. Zircon textures and composition: refractory recorders of magmatic volatile evolution? Contrib. Mineral. Petrol. 165 (1), 45–71.
Erdmann, S., Martel, C., Pichavant, M., Kushnir, A., 2014. Amphibole as an archivist of magmatic crystallization conditions: problems, potential, and implications for inferring magma storage prior to the paroxysmal 2010 eruption of Mount Merapi, Indonesia. Contrib. Mineral. Petrol. 167, 1016–1038.
Frost, B.R., Barnes, C.G., Collins, W.J., Arculus, R.J., Ellis, D.J., Frost, C.D., 2001. A geochemical classification for granitic rocks. J. Petrol. 42 (11), 2033–2048.
Hammarstrom, J.M., Zen, E.-A., 1986. Aluminium in hornblende: an empirical igneous geobarometer. Am. Mineral. 71 (1), 1297–1313.
Hammarstrom, J.M., Zen, E.-A., 1992. Discussion of Blundy and Holland's (1990) "Calcic amphibole equilibria and a new amphibole–plagioclase geothermometer". Contrib. Mineral. Petrol. 111 (2), 264–268.
Harlov, D.E., Van Den Kerkhof, A., Johansson, L., 2013. The Varberg–Torpa charnockite–granite association, SW Sweden: mineralogy, petrology, and fluid inclusion chemistry. J. Petrol. 54 (1), 3–40.
Hawthorne, F.C., Oberti, R., Harlow, G.E., Maresch, W.V., Martin, R.F., Schumacher, J.C., Welch, M.D., 2012. IMA report. Nomenclature of the amphibole supergroup. Am. Mineral. 97 (11–12), 2031–2048.
Holland, T., Blundy, J., 1994. Non-ideal interactions in calcic amphiboles and their bearing on amphibole–plagioclase thermometry. Contrib. Mineral. Petrol. 116 (1), 433–447.
Hollister, L.S., Grissom, G.C., Peters, E.K., Stowell, H.H., Sisson, V.B., 1987. Confirmation of the empirical correlation of Al in hornblende with pressure of solidification of calc-alkaline plutons. Am. Mineral. 71, 231–239.
Holtz, F., Becker, A., Freise, M., Johannes, W., 2001. The water-undersaturated and dry Qz–Ab–Or system revisited. Experimental results at very low water activities and geological implications. Contrib. Mineral. Petrol. 141, 347–357.
Huang, F., Scaillet, B., Wang, R., Erdmann, S., Chen, Y., Faure, M., Liu, H., Xie, L., Wang, B., Zhu, J., 2019. Experimental Constraints on Intensive Crystallization Parameters and Fractionation in A-Type Granites: A Case Study on the Qitianling Pluton, South China. Journal of Geophysical Research: Solid Earth 124. https://doi.org/10.1029/2019JB017490.
Johnson, C.M., Czamanske, G.K., Lipman, P.W., 1990. H, O, Sr, Nd, and Pb isotope geochemistry of the Latir volcanic field and cogenetic intrusions, New Mexico, and relations between evolution of a continental magmatic center and modifications of the lithosphere. Contrib. Mineral. Petrol. 104 (1), 99–124.
Johnson, M.C., Rutherford, M.J., 1989. Experimental calibration of the aluminum-in-hornblende geobarometer with application to Long Valley caldera (California) volcanic rocks. Or. Geol. 17 (9), 837–841.
King, P.L., Sham, T.-K., Gordon, R.A., Dyar, D., 2013. Microbeam X-ray analysis of Ce^{3+}/Ce^{4+} in Ti-rich minerals: a case study with titanite (sphene) with implications for multivalent trace element substitution in minerals. Am. Mineral. 89 (1), 110–119.
Leake, B.E., Wooley, A.R., Arps, C.E.S., Birch, W.D., Gilbert, M.C., Grice, J.D., et al., 1997. Nomenclature of amphiboles; report of the subcommittee on amphiboles of the international mineralogical association commission on new minerals and mineral names. Am. Mineral. 82 (9), 1019–1037.
Lipman, P.W., 2007. Incremental assembly and prolonged consolidation of Cordilleran magma chambers: evidence from the Southern Rocky Mountain volcanic field. Geosphere 3 (1), 42–70.
Markl, M., Piazolo, S., 1999. Stability of high-Al titanite from low-pressure calcsilicates in light of fluid and host-rock composition. Am. Mineral. 84 (1–2), 37–47.
Mesquita, C.J.S., Dall'Agnol, R., Almeida, J.A., 2018. Mineral chemistry and crystallization parameters of the A-type Paleoproterozoic Bannach granite, Carajás province, Pará, Brazil. Braz. J. Geol. 48 (3), 575–601.
Morad, S., El-Ghali, M.A.K., Caja, M.A., Al-Ramadan, K., Mansurbeg, H., 2009. Hydrothermal alteration of magmatic titanite: evidence from Proterozoic granitic rocks, Southeastern Sweden. Can. Mineral. 47 (4), 801–811.
Mutch, E.J.F., Blundy, J.D., Tattitch, B.C., Cooper, F.J., Brooker, R.A., 2016. An experimental study of amphibole stability in low-pressure granitic magmas and a revised Al-in-hornblende geobarometer. Contrib. Mineral. Petrol. 171, 85.
Oberti, R., Smith, D.C., Rossi, G., Caucia, F., 1991. The crystal-chemistry of high-aluminum titanites. Eur. J. Mineral. 3, 777–792.
Pan, L.-C., Hu, R.-Z., Bi, X.-W., Li, C., Wang, X.-S., Zhu, J.-J., 2018. Titanite major and trace element compositions as petrogenetic and metallogenic indicators of Mo ore deposits: examples from four granite plutons in the southern Yidun arc, SW China. Am. Mineral. 103 (9), 1417–1434.
Putirka, K., 2016. Amphibole thermometers and barometers for igneous systems and some implications for eruption mechanisms of felsic magmas at arc volcanoes. Am. Mineral. 101 (4), 841–858.
Scaillet, B., Holtz, F., Pichavant, M., 2016. Experimental constraints on the formation of silicic magmas. Elements 12 (2), 109–114.
Scaillet, B., Pichavant, M., Roux, J., 1995. Experimental crystallisation of leucogranite magmas. J. Petrol. 36 (3), 663–705.
Schmidt, M.W., 1992. Amphibole composition in tonalite as a function of pressure; an experimental calibration of the Al-in-hornblende barometer. Contrib. Mineral. Petrol. 110 (2–3), 304–310.
Schumacher, J.C., 1997. Appendix 2: the estimate of ferric iron in electron microprobe analysis of amphiboles. Eur. J. Mineral. 61 (405), 643–651.
Shu, X.-J., Wang, X.-L., Sun, T., Xu, X., Dai, M.-N., 2011. Trace elements, U–Pb ages and Hf isotopes of zircons from Mesozoic granites in the western Nanling Range, South China: implications for petrogenesis and W–Sn mineralization. Lithos 127 (3–4), 468–482.
Smith, D.C., 1981. The pressure and temperature dependence of Al-solubility in sphene in the system Ti-Al-Ca-Si-O-F. Progr. Exp. Petrol., Series D 18, 193–197.
Solgadi, F., 2010. Origine et développement de litages dans des roches de composition granitique. Ph. D thesis. Université de Chicoutimi, Québec, Canada, pp. 1–486.
Storey, C., Jeffries, T., Smith, M., 2006. Common lead-corrected laser ablation ICP–MS U–Pb systematics and geochronology of titanite. Chem. Geol. 227 (1–2), 37–52.
Stussi, J.-M., Cheilletz, A., Royer, J.-J., Chevremont, P., Feraud, G., 2002. The hidden monzogranite of Soultz-sous-Forêts (Rhine Graben, France). Géologie de la France 1, 45–64.
Sun, J.-F., Wu, F.-Y., Xie, L.-W., Yang, Y.-H., Liu, Z.-C., Li, X.-H., 2012. In situ U–Pb dating of titanite by LA-ICPMS. Chin. Sci. Bull. 2506–2516.
Toulmin III, P., Hammarstrom, J., 1990. Geology at the Mount Aetna volcanic center, Chaffee and Gunnison counties, Colorado. USGS Bull., p. 44
Tropper, P., Manning, C.E., Essene, E.J., 2002. The substitution of Al and F in titanite at high pressure and temperature: experimental constraints on phase relations and solid solution properties. J. Petrol. 43 (10), 1787–1814.
Wang, R.C., Xie, L., Chen, J., Yu, A., Wang, L., Lu, J., Zhu, J., 2013. Tin-carrier minerals in metaluminous granites of the western Nanling Range (southern China): constraints on processes of tin mineralization in oxidized granites. J. Asian Earth Sci. 74, 361–372.
Wang, Z., Chen, B., Ma, X., 2014. Petrogenesis of the Late Mesozoic Guposhan composite plutons from the Nanling range, South China: implications for W–Sn mineralization. Am. J. Sci. 314 (1), 235–277.
Wang, G.-C., Jiang, Y.-H., Liu, Z., Ni, C.-Y., Qing, L., Zhang, Q., Zhu, S.-Q., 2016. Multiple origins for the Middle Jurassic to Early Cretaceous high-K calc-alkaline I-type granites in northwestern Fujian province, SE China and tectonic implications. Lithos 246–247, 197–211.
Whitney, D.L., Evans, B.W., 2010. Abbreviations for names of rock-forming minerals. Am. Mineral. 95 (1), 185–187.
Xie, L., Wang, R.C., Chen, J., Zhu, J.C., 2010. Mineralogical evidence for magmatic and hydrothermal processes in the Qitianling oxidized tin-bearing granite (Hunan, South China): EMP and (MC)-LA-ICPMS investigations of three types of titanite. Chem. Geol. 276 (1–2), 53–68.

Zhang, J., Humphreys, M.C.S., Cooper, G.F., Davidson, J.P., Macpherson, C.G., 2017. Magma mush chemistry at subduction zones, revealed by new melt major element inversion from calcic amphiboles. Am. Mineral. 102 (6), 1353–1367.

Zhao, K.-D., Jiang, S.-Y., Jiang, Y.-H., Wang, R.-C., 2005. Mineral chemistry of the Qitianling granitoid and the Furong tin ore deposit in Hunan province, South China. Eur. J. Mineral. 17 (4), 635–648.

Zhu, J.-J., Richards, J.P., Rees, C., Creaser, R., DuFrane, S.A., Locock, A., Petrus, J.A., Lang, J., 2018. Elevated magmatic sulfur and chlorine contents in ore-forming magmas at the Red Chris porphyry Cu–Au deposit, Northern British Columbia, Canada. Econ. Geol. 113 (5), 1047–1075.